# Stability of Statics Aware Voronoi Grid-Shells

D. Tonelli[a,*], N. Pietroni[b], E. Puppo[c], M. Froli[a], P. Cignoni[b], G. Amendola[d], R. Scopigno[b]

[a] *University of Pisa, Faculty of Engineering, Dept. DESTeC, Pisa - Italy*
[b] *VCLab, CNR-ISTI, Pisa - Italy*
[c] *University of Genova, Faculty of Engineering, Dept. Dibris, Genova - Italy*
[d] *University eCampus, Via Isimbardi 10 - 22060 Novedrate (CO) - Italy*

---

**Abstract**

Grid-shells are lightweight structures used to cover long spans with few load-bearing material, as they excel for lightness, elegance and transparency. In this paper we analyse the stability of hex-dominant free-form grid-shells, generated with the *Statics Aware Voronoi Remeshing* scheme introduced in (1). This is a novel hex-dominant, organic-like and non uniform remeshing pattern that manages to take into account the statics of the underlying surface. We show how this pattern is particularly suitable for free-form grid-shells, providing good performance in terms of both aesthetics and structural behaviour. To this end, we select a set of four contemporary architectural surfaces and we establish a systematic comparative analysis between Statics Aware Voronoi Grid-Shells and equivalent state of the art triangular and quadrilateral grid-shells. For each dataset and for each grid-shell topology, imperfection sensitivity analyses are carried out and the worst response diagrams compared. It turns out that, in spite of the intrinsic weakness of the hexagonal topology, free-form Statics Aware Voronoi Grid-Shells are much more effective than their state-of-the-art quadrilateral counterparts. Eventually, we show the results of incremental load tests performed on a physical mock-up of a Statics Aware Voronoi Grid-Shell.

*Keywords:*
Grid-shells, topology, Voronoi, free-form, imperfection sensitivity, buckling, equivalent continuum, mock-up

*Corresponding author
*Email address:* `davide.tonelli@dic.unipi.it` (D. Tonelli)

## 1. Grid-shells: topology and stability

Grid-shells, also called lattice shells or reticulated shells, belong to the category of *lightweight structures*. The shape of these structures is optimized to support its own weight, its geometry being modified to provide additional stiffness to the overall structure. Unfortunately, they are as efficient as exposed to risky buckling phenomena. In terms of structural behaviour, grid-shells indeed share some traits with their 'brothers' shells, but at the same time they are lighter and more flexible, hence even harder to analyse than proper shells.

Shells typically suffer from modes interaction (i.e. some of the first linear buckling factors are coincident or have little separation) and imperfection sensitivity (i.e. a slight perturbation of their curvature may produce an unexpected deterioration of their static behaviour). Both these phenomena are extremely detrimental and usually lead to a huge abatement of the theoretical linear buckling load of the perfect shell (2; 3).
Although grid-shells are much more efficient than 'equivalent' shells with the same weight and span (because the material distribution is more efficient), luckily for them the aforementioned phenomena are less pronounced, although still present and indeed dangerous (4). This is because the collapse load is more likely to be determined by limit point rather than by bifurcation

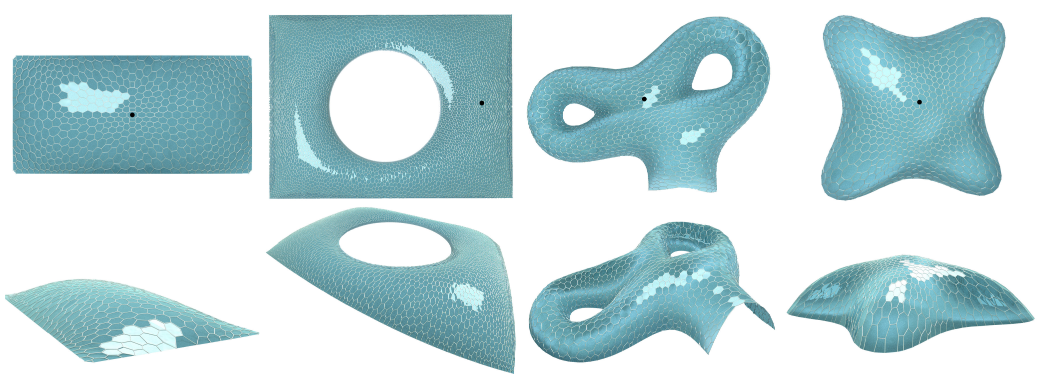

Figure 1: All Datasets. From left to right respectively: *Neumünster Abbey* glass roof, *British Museum* great court glass roof, *Aquadom* and *Lilium Tower* architectural free form shapes. The black bullet is the state parameter adopted in the geometrically nonlinear analyses.

of equilibrium. Nonetheless, the failure mode is mainly influenced by the grid topology, and section 6.1 shows how usually an unstable symmetric bifurcation point appears associated with triangular topology and quasi-funicular underlying surface with regular boundary.

Analytical relationships are available for the calculation of the linear buckling load for shells of some shapes and restraint conditions (5), together with experimental knockdown factors for abating the linear unsafe values (6), as a result of the efforts of theoretical and industrial research carried out since the end of the XIX century. Unfortunately, no akin results are available for grid-shells. Some attempts were done for evaluating the equivalent membrane stiffness and thickness of planar grids, in order to estimate the buckling load of grid-shells by using the available relationships for continuous shell (7; 8). Although overestimating the real buckling load and totally disregarding imperfections and material non-linearity (9; 4), the equivalent continuum method is very useful at least in the preliminary phase of the assessment process. Unfortunately, analytical solutions are available for a finite number of continuum shells, thus limiting its application. As a consequence, fully non-linear numerical analyses are the standard tool for the assessment of the stability of grid-shells.

From a geometrical point of view, grid-shells can be considered as the discretization of continuous shells: the continuous shape is tessellated by a set of connected piecewise linear modules composing a manifold mesh. It is evident that both curvature and meshing influence the statics of the structure, but while the effect of curvature can be somehow envisaged with the theory of shells (5), the outcome of meshing is much more difficult to predict and additionally few related references are available (10, p. 239-244). Summarily, the behaviour of a grid-shell is utterly affected by the *Gaussian curvature* of its underlying surface, the *grid topology*, the *grid spacing*, the *beam cross section*, the *joint stiffness* and the (potential) *stiffening method* (11; 4).

Up to now, many examples of glass covered grid-shells have been built, the vast majority of which being designed with triangular and quadrilateral grid topologies (12; 13; 14). Triangular grid-shells are unanimously credited as the most statically efficient structures as they rely on extensional deformation only, whereas quadrilateral grid-shells provide a better trade-off between statics efficiency, transparency and manufacturing cost. In fact, quadrilaterals achieve high transparency at equal weight, as their *area/perimeter* ratio is higher than that provided by triangles. Additionally, planar panels can be easily obtained that, by virtue of their almost right angles, are easier and cheaper to produce than triangular panels (15; 16). Unfortunately, quadrilateral and polygonal patterns generally undergo 'inextensional deformation' (i.e. that involves beams bending), that makes them less efficient than their triangular competitors. As a consequence, most frequently the effective use of the quadrilateral topology required the adoption of special stiffening methods (e.g. bracing cables) (17), whereas 'higher order' topologies such as the hexagonal one are yet highly mistrusted by structural engineers. This attitude is not totally fair because, while hexagonal grids display an isotropic equivalent mechanical behaviour, quadrilateral grids are orthotropic and it is demonstrated that their efficiency greatly varies with the loading direction, becoming even much worse than that of hexagons in the most unfavourable case (18). This in turn indicates that a grid-shell with an optimized Voronoi-like topology (i.e. hex-dominant), might display a very satisfying structural behaviour.

Indeed, in this paper we focus on pinning down the structural behaviour of Statics Aware Voronoi Grid Shells introduced in (1), that are actually polygonal hex-dominant grid-shell structures, i.e. composed of mostly hexagonal faces, including a few generic polygonal faces, usually heptagons, pentagons and quads. From a purely geometric viewpoint, this kind of structures turns out to be extraordinarily *adaptive* and suitable for *free form architecture*, definitely much more than purely hexagonal structures (19). In the following, we demonstrate how this pattern can be successfully used to tessellate *highly free form surfaces* providing static performances that are considerably better than current practice quadrilateral remeshing schemes, while for quite *regular* geometries the performances are comparable. This also demonstrates how the *'statics awareness'* introduced in (1) can be adopted to overcome the intrinsic structural weakness of polygonal topologies.
As a last remark it is worth noting that, for the sake of brevity, in the proposed experiments we considered no stiffening method (e.g. bracing cables).

## 2. Stability checks for grid-shells

Grid-shells are compressive structures and consequently they can display several types of stability failure (4; 20):

1. **member buckling:** the classic Euler beam buckling under concentric axial load;

2. **node instability:** a set of beams fails locally due to the snap through of a node;
3. **line instability:** all nodes of a ring in a dome or a generatrix of a barrel vault buckle simultaneously (less determinant for free-form shapes);
4. **global instability:** the whole structure undergoes sudden long-wave displacements.

Usually member instability is decisive for high grid spacing values, whereas global instability and line instability are more likely to appear in conjunction with dense networks (4). However, instabilities of type 1, 2 and 3 cannot be oberved by using simple cells, simplified static schemes or the equivalent continuum method. Therefore, in the general case, the assessment of the load bearing capacity of a grid-shell relies on performing numerical non-linear buckling analyses: the so called 'direct' method. In particular, the Finite Element Analysis (FEM) proves to be very effective as it allows to model any generic situation:

- it allows to analyse any shape, also free-form shapes;
- it makes it possible to point out buckling of all types;
- it allows to take into account the effect of imperfections;
- it allows to observe the softening behaviour (geometrical non-linearity);
- it allows to introduce material non-linearity.

Therefore we performed systematic geometrically non-linear numerical analyses with a commercial FEM software (21). Details are given in section 5.1. In particular, we chose not to consider material non-linearity because of the higher computational time needed and the large number of analyses performed. Indeed it is likely that the failure mode of grid-shells, especially if free-form, would be affected by yielding of the beams material (as is the case for the British Museum Great Court roof, for example). But the purpose of this study is not that of assessing the real buckling load of a design grid-shell, but instead only that of estimating the buckling strength of the Statics Aware Voronoi Grid-Shells in comparison with their state-of-the-art competitors. For this reason, we have deemed geometrically non-linear analyses to be accurate enough for our aim.

## 3. Iimperfection sensitivity analysis

It is well-known that the solution of the generalized eigenvalue problem:

$$det(\mathbf{K}) = det(\mathbf{K}_e + \lambda \mathbf{K}_\sigma) = 0 \tag{1}$$

where $\mathbf{K}$ is the initial global stiffness matrix, $\mathbf{K}_e$ is the initial global elastic stiffness matrix, $\mathbf{K}_\sigma$ is the global geometric stiffness matrix and $\lambda$ is the load factor that amplifies the external loads, provides an overestimate of the real buckling load. This is especially the case for shells and grid-shells endowed with a high level of symmetry, where imperfection sensitivity and modes buckling interaction may even halve the theoretical buckling load (3). This happens because these kinds of structures are characterized by a high share of membrane strain energy compared to the bending strain energy, and this in turn makes them very sensitive to imperfections (22). The process of evaluating the effects of imperfections on the buckling strength of a structure is known as imperfection sensitivity analysis, and it is essential in assessing the safety of efficient structures.

Koiter (2) elaborated the'initial post-buckling theory', which assumes that it is possible to evaluate the behaviour of the imperfect structure by knowing the behaviour of the perfect one. It applies to structures showing bifurcation of equilibrium and lays its foundations on the asymptotical approximation of the post-buckling path. Unfortunately, it is limited to almost linear fundamental paths only as well as imperfections of small amplitude.

A more recent trend is the 'mimimum perturbation energy' concept, which identifies snap-through phenomena towards secondary equilibrium paths by perturbing the system (23; 24).

Nevertheless, the most commonly adopted method for determining the effect of imperfections is that of numerically analysing the imperfect model itself, which is called under the name of 'direct approach'. This in turn raises the question of how to compute the 'worst imperfection', i.e. that imperfection that yields the lower buckling factor. It is worth noticing that the problem of finding the worst imperfection shape within a given amplitude limit is also coupled in the variables shape and amplitude. This search is still an open problem and some even think it does not have a unique solution (25). Indeed this approach has the advantage that complex searches for the non-linear post-critical path are avoided, as the introduction of the imperfections converts bifurcation points into limit points. On the other hand, it is definitely computationally expensive as it requires to carry out a series of fully non-linear analyses on a (possibly infinite) set of models adulterated with different imperfections. The computational cost is sometimes discouraging, especially for everyday design. As a consequence, several variations to the general procedure have been proposed.

Deml and Wunderlich (26) propose to describe imperfections as additional nodal degrees of freedom and to solve for both the buckling load and the corresponding "worst" imperfection shape by solving an extended system of nonlinear equations.

After the studies of Ho (27) it was known that the worst imperfection shape is to be sought after within the convex linear combinations of the linear eigenmodes (i.e. the eigenvectors $\mathbf{u}_i$ associated to the solutions $\lambda_i$ of equation (1), with $\mathbf{u}_i^T\mathbf{u}_j = \delta_{ij}$). Subsequently it was also observed that in certain cases, especially when the softening behaviour is much pronounced in the pre-buckling phase, the worst imperfection shape must also take into account the non-linear eigenmodes (i.e. the he eigenvectors $\mathbf{u}_i$ associated to the solutions $\lambda_i$ of equation (1), with $\mathbf{K}$ being evaluated just before the bifurcation point) (28).

A modern approach of absorbing this knowledge is that of setting up a non-linear optimization problem in which the solution is sought within convex linear combinations of linear and non-linear eigenmodes, subjected to user-defined imperfection amplitude constraints, by minimizing the buckling load (29). As expected, it is found out that lower buckling loads are obtained by considering also non-linear buckling modes and that the worst imperfection shape is usually composed of several eigenmodes. Additionally, it is noticed that the first non-linear eigenmode is a very good approximation of the worst imperfection shape. Nevertheless, it is also common knowledge that the first linear eigenmode represents a satisfactory approximation as well (30), although for some structures higher linear eigenmodes might erode the load bearing capacity even more (31).

Kristanic and Korelc (32) propose instead a linear optimization problem, by carefully choosing linear constraints on both the shape and the amplitude of the imperfections. They also include deformation shapes (i.e. the displacement fields of the structure due to relevant load cases) among the base shapes for the generation of the convex linear combinations.

However, other studies showed that the worst imperfection form depends on the specific combination of structure's geometry and loading. Additionally, dimples and local imperfections in general that are more relevant to production and may also represent the occurrence of local instabilities along the

loading path, might also cater for the maximum reduction in load bearing capacity (33; 34).Therefore, eigenmodes combinations as well as all long-wave imperfections may overestimate the buckling load.It is also worth noticing that some authors include also several post-buckling deformed shapes among the competitors for the worst imperfection shape (33; 35).
As a consequence of this knowledge, the concept of 'quasi-collapse-affine imperfection' has emerged, together with the awareness that the worst imperfection shape cannot be pinpointed (25). Schneider finds that the worst imperfection pattern does not exist for shells because it depends on the imperfection amplitude. Additionally, it cannot be spotted as it relies heavily on clustering of instability loads, crossing of secondary equilibrium paths in the post-buckling range and material non-linearity. Therefore he introduces the concept of 'quasi-collapse-affine imperfections': displacement fields extracted from the initial stage of the buckling process, obtained by conveniently restricting the space of the shape functions. These imperfections turn out to be more unfavourable than eignemodes, especially when the instability is caused also by material non-linearity. Actually they initiate the buckling process (they 'stimulate' it) and thus they allow to approach the most unfavourable imperfection pattern (35).

Most of the described contributions are specific to shells, whereas few references specific to grid-shells are available. Bulenda and Knippers (20) propose to adopt as imperfection shapes the non-linear eigenmodes and the displacement shapes of the grid-shell under relevant load cases.
We use GSA as a FE-program (21), a commercial software which does not allow the user to check and manipulate the stiffness matrix. Thus we cannot neither obtain non-linear eigenmodes nor restrict the space of the shape functions in order to compute 'virtual' initial buckling shapes (as proposed by Schneider (35)). However, our study is a parametric analysis on the imperfection sensitivity of grid-shells with different topology (i.e., triangular, quadrilateral and hex-dominant), and not a thorough assessment of the safety of real projects. All this being said, we content ourselves with 'stimulating' the buckling process as proposed by Schneider (25; 35), by adopting the following imperfections shapes (see Figure 2 for an example):

1. the displacement shape obtained by linear static analysis, addressed with the acronym $LS$ in the following;
2. the initial buckling shape obtained by geometrically non-linear analysis

(i.e. the 'real quasi-collapse-affine' imperfection according to Schneider (25; 35)), addressed with the acronym *NLS* in the following;

3. the first linear eigenmode and convex linear combinations of the first ten linear eigenmodes, addressed with the acronym *LB* in the following. No optimization procedure is established: the generic $i$-th buckling mode is included when a visual resemblance is noticed with the non-linear initial buckling shape of the grid-shell (i.e. *NLS*).

It is worth noticing once again that, as this is a comparative analysis and not a real project, only the uniformly distributed load case has been considered. No asymmetric load cases have been addressed, neither in the buckling analyses nor in the definition of the imperfection shapes.
For each dataset (see Table 1), for each topology and for each imperfection shape, we have created a range of imperfect models by varying the norm of the imperfections and its sign. The norm is Euclidean ($||\mathbf{e}||_2 = \sqrt{\sum_i (e_{ix}^2 + e_{iy}^2 + e_{iz}^2)}$) and it was sampled at regulars intervals $\pm[250\ 200\ 150\ 100\ 50\ 25\ 0]$ mm. Every time the imperfections shapes have been scaled according to the selected maximum norm and added to the perfect geometry. We have also taken into account the sign of the imperfections, as it may significantly influence the buckling behaviour of the grid-shell.
In doing so, we ended up with a total of 13 imperfect models for each imperfection shape, for each topology and for each dataset, for a total of more than 400 models (see second column of Table 1). Each model has then been analysed with the GSA FE-program (21), by carrying out geometrically non-linear buckling analyses (see section 2 for reasons about neglecting material non-linearity and section 5.1 for details about modeling and load cases). Imperfection sensitivity diagrams are shown in Figure 6, whereas relevant load-deflection diagrams are displayed in Figure 7.

## 4. Statics aware Voronoi remeshing

Here we briefly report the method we use to design the Statics Aware Voronoi Grid-Shells. Our method is based on *Anisotropic Centroidal Voronoi Tessellations (ACVT)* (36) and it is driven by the statics of the input surface, aiming at improving the strength of the grid-shell as well as its aesthetics.

Voronoi diagrams appear in nature in many forms. In several cases, such as in the porous structure of animal bones, Voronoi-like structures optimize strength while keeping a light weight. We follow a similar approach to design

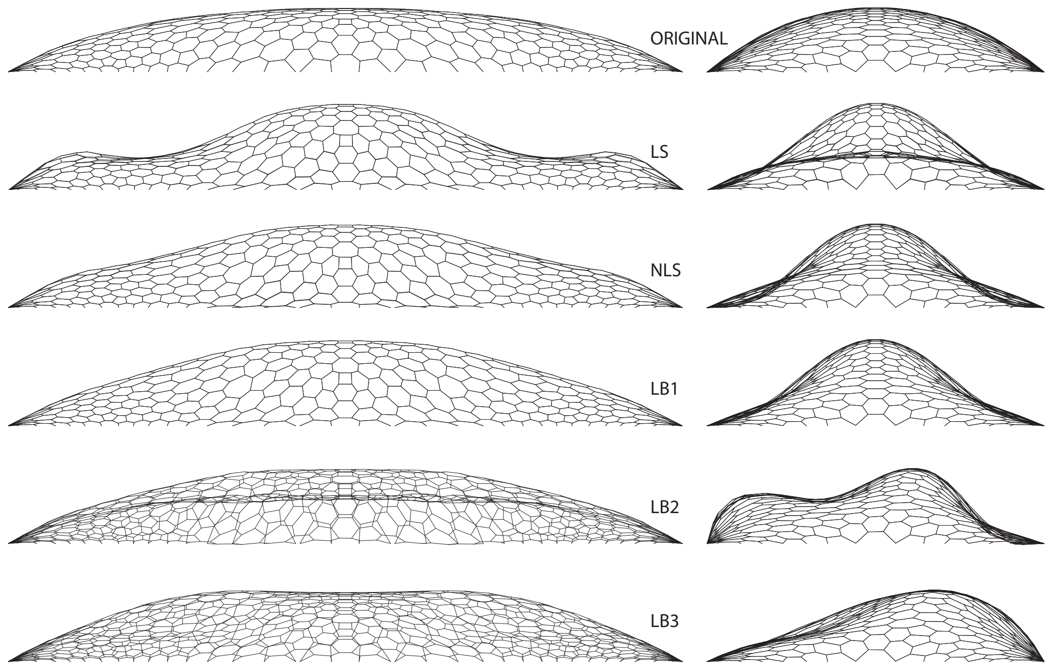


Figure 2: Magnified deformed shapes for the hex-dominant remeshing of the Neumünster dataset, side and front views. From top to bottom respectively: ORIGINAL, LS, NLS, 1st LB eigenmode, 2nd LB eigenmode and 3rd LB eigenmode.

hex-dominant grid-shells, by concentrating more cells of smaller size in zones subject to higher stress, while aligning the elements of our grid to the maximum stress direction. The pipeline of the method is summarised in Figure 3 and briefly discussed below. The reader is referred to (1) for further details.

Given an initial surface $\Sigma$, we first perform a linear static analysis of the continuous shell (we always consider a uniformly distributed load case, but in theory every load condition can be adopted), thus obtaining a stress tensor for each point $p \in \Sigma$. As a thin shell can be considered in a plane stress condition, the resulting stress tensor is two-dimensional. Therefore we express it with respect to the local principal directions and we represent it as a pair of mutually orthogonal line fields[1] $\Psi(p) = (\vec{u}(p), \vec{v}(p))$, where $\vec{u}$ and $\vec{v}$ define the maximum and minimum principal stresses at each point of the

[1]A line field is a vector field modulo its orientation: only the directions and sizes of $\vec{u}$ and $\vec{v}$ are relevant to $\Psi$, not their orientations.

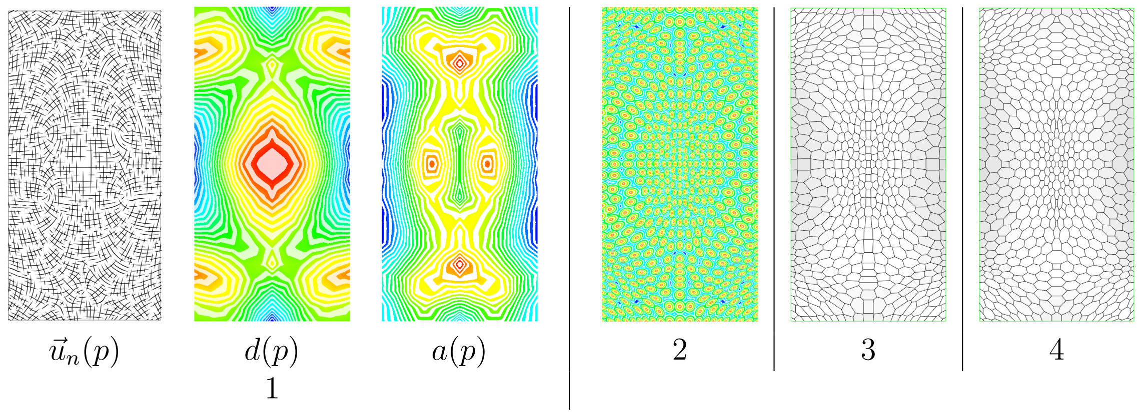


Figure 3: The different steps composing the pipeline of (1): the components of the stress tensor inducing the anisotropic metric (1); the distribution of seeds and their distance field (2); the corresponding ACVT (3); the final optimized tessellation (4).

surface, respectively. Since $\vec{u}$ and $\vec{v}$ are orthogonal, we decouple the scalar and directional information and represent $\Psi$ as a triple $(\vec{u}_n(p), d(p), a(p))$, where $\vec{u}_n$ is a unit-length vector parallel to $\vec{u}$, $d = |\vec{u}|$ is the maximum stress intensity (henceforth called *density*), and $a = |\vec{u}|/|\vec{v}|$ is the *anisotropy* (see Figure 3.1). Tensor $\Psi$ induces an anisotropic metric $g_\Psi = \mathrm{diag}(\frac{1}{d^2}, \frac{a^2}{d^2})$ on surface $\Sigma$, where the matrix is expressed with respect to the principal reference system at $p$.

Next we compute a hex-dominant tessellation covering $\Sigma$, whose faces have a uniform distribution with respect to metric $g_\Psi$. Roughly speaking, this means that faces will be more dense where the maximum stress is higher and they will be elongated along the direction of maximum stress proportionally to anisotropy.

In order to do so, we sample a set of seeds on the surface (37), and then we relax their positions, so that the distribution of seeds becomes uniform with respect to metric $g_\Psi$. Relaxation consists of computing the Voronoi diagram of the seeds under metric $g_\Psi$ and iteratively moving each seed to the centroid of its Voronoi cell (38), until convergence. Note that, since $g_\Psi$ has variable density and is anisotropic, the distribution of seeds will not be uniform with respect to the Euclidean metric: Figure 3.2 depicts the distribution of seeds (red dots) together with the corresponding field that encodes distance of points on the surface from the seeds; Figure 3.3 depicts the corresponding ACVT, which assembles the (anisotropic) Voronoi cells of all seeds and is easily computed from the distance field.

| Dataset | Model | Vertices' Valence | Vertices | Faces | Edges | Beams' section (mm) | Total length (m) |
|---|---|---|---|---|---|---|---|
| *Neumünster Abbey* | Triangular (39) | 6 | 220 | 380 | 541 | CS $\phi$ 60 | 966.7 |
| | Quadrilateral | 4 | 508 | 464 | 883 | CS $\phi$ 60 | 932.7 |
| | Voronoi | 3 | 1076 | 553 | 1522 | CS $\phi$ 60 | 956.9 |
| *British Museum* | Triangular (40) | 6 | 1746 | 3312 | 4878 | CHS 120x30 | 10267.4 |
| | Quadrilateral | 4 | 4693 | 4452 | 8723 | CHS 120x30 | 10184.8 |
| | Voronoi | 3 | 10221 | 5784 | 14829 | CHS 120x30 | 10316.6 |
| *Aquadom* | Quadrilateral (41) | 4 | 1078 | 1001 | 1936 | CHS 100x20 | 3672.1 |
| | Voronoi | 3 | 2382 | 1189 | 3400 | CHS 100x20 | 3662.3 |
| *Lilium Tower* | Quadrilateral (41) | 4 | 665 | 636 | 1244 | CHS 100x20 | 2139.9 |
| | Voronoi | 3 | 1432 | 717 | 2060 | CHS 100x20 | 2121.1 |

Table 1: Statistics on datasets. When a reference is given the remeshing comes from that source, otherwise it is a height field isotropic remeshing $s(x, y)$.

Finally, we apply geometric optimization to improve the local shape of the faces of the hex-dominant mesh. Roughly speaking, we deform each face to its closest regular polygon under metric $g_\Psi$ and we globally optimise the mesh by stitching adjacent polygons. The result of optimisation is depicted in Figure 3.4.

## 5. Experimental setup

We have tested our method on several input surfaces. Figure 1 shows the rendered views of the hex-dominant remeshing of these surfaces (i.e. the Statics Aware Voronoi Grid-Shells), whereas Figure 4 compares the top views of the various remeshings of each input surface. A summary of the datasets is presented in Table 1:

1. *Neumünster Abbey* is the glass roof of the courtyard of the Neumünster Abbey in Luxembourg, designed by RFR-Paris (39) and built in 2003;
2. *British Museum* is the great court glass roof in the British Museum: geometry rationalization by Prof. Chris J. K. Williams (40), structural design by Buro Happold and construction completed in 2000 by Waagner Biro;
3. *Aquadom* and *Lilium Tower* are architectural free form shapes; the latter is the top of the Lilum Tower skyscraper designed by Zaha Hadid

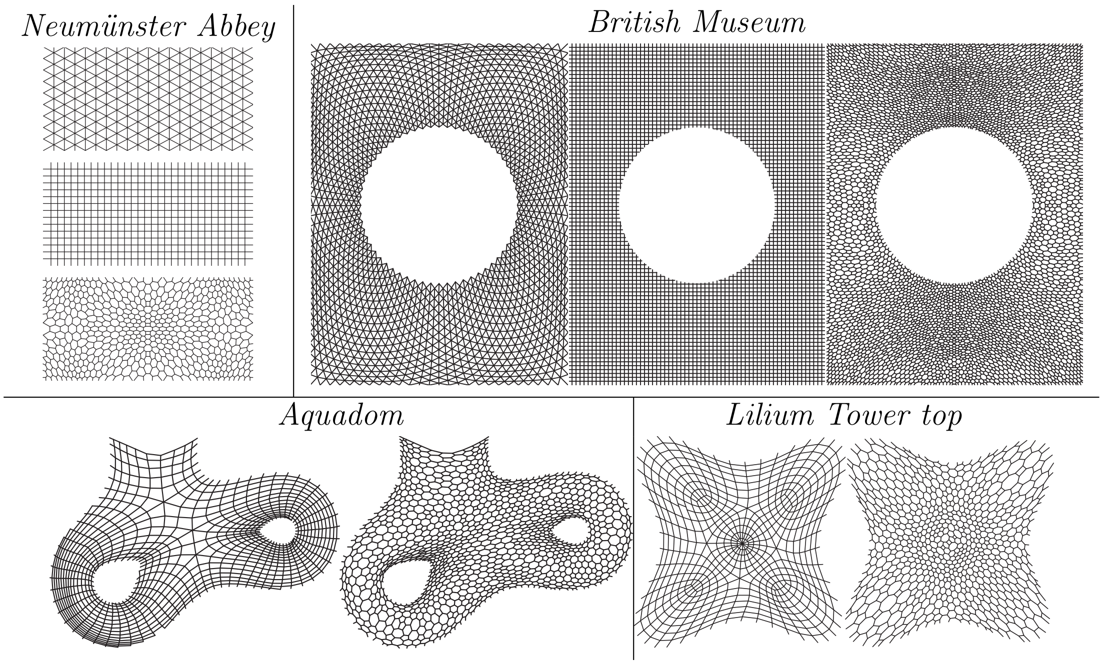


Figure 4: Top views of all remeshings utilised in our comparative analysis.

architects. The quadrilateral remeshings for these datasets comes from the statics optimization procedure of (41).

*Neumünster* and *British Museum* datasets represent lightweight, quite ordinary surface geometries and very low height-to-span ratio grid-shells, whereas *Aquadom* and *Lilium Tower* embody architectural free form skins as well as high height-to-span ratio grid-shells.

### *5.1. Restraints, load conditions, numerical modeling*

Since this is a comparative analysis and not a specific study on the topic of stability of grid-shells, some simplifications have been done:

1. All models have *pin joints* all over the boundary;
2. The section of beams varies according to the specific model (as is shown in Table 1) but it is constant within each model;
3. The load is always uniformly distributed. There are three load cases, respectively:
   (a) $G_1$ which is the dead load of the beams;

(b) $G_2$ which is a uniform load of 0.75 $kN/m^2$ of magnitude, that stands for an hypothetical 25 mm thick glass coverage;

(c) $Q_k$ which is a uniform load of 1.00 $kN/m^2$ of magnitude, that represents the snow action.

Then a load combination only $q = 1.0G_1 + 1.0G_2 + 1.0Q_k$, which is representative of the characteristic serviceability load, is used to carry out all the analyses;

4. Material non-linearity is neglected as the analyses already involves many variables (see section 2 for explanation);
5. Each beam is modeled as a single finite element in order to reduce the computational time, while keeping an acceptable level of accuracy of the overall simulation. This simplification prevents form pointing out single member buckling, but it is still acceptable as member buckling is not the ordinary failure mode for grid-shells.

### *5.2. Statics comparison criteria*

As we want to assess the structural performances of the Statics Aware Voronoi Grid-Shells, we set up a comparative evaluation with respect to other current practices (e.g. triangular and quadrilateral remeshing schemes).
As roughly stated by Gioncu (4) and Malek (11), the structural performance of a grid-shell with fixed topology is not only affected by the total weight of its members but also by the grid-spacing. Figure 5 shows the results of grid-spacing sensitivity analysis carried out on a shallow spherical cap (60 m of span and 2.8 m of height) remeshed with triangular, quadrilateral and our statics aware Voronoi-like topologies, respectively, keeping the total mass constant. It is evident that the constancy of the total structural mass (i.e. the total weight of the beams) is not a satisfactory comparison criterion, as the load bearing capacity of some grid-shells (i.e. those with triangular topology) greatly varies with the grid-spacing. Therefore, it is found out that the constancy of both total structural mass and total length of the beams is an adequate statics comparison criterion.
As a consequence, for each dataset and for each topology, each remeshing was generated with the same overall length (see last column of Table 1 - we tolerate a 5% of variation) and with the same beams' diameter (which means that also the total weight keeps constant).

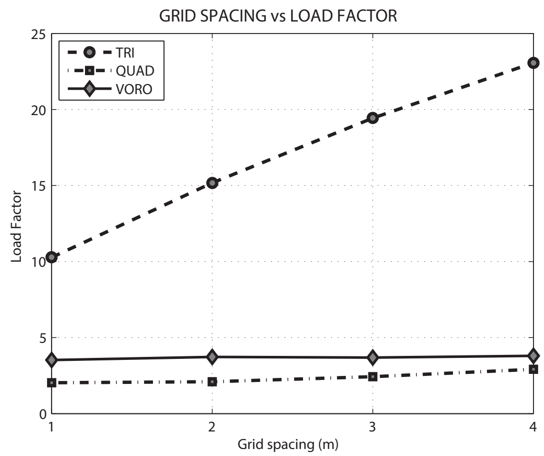


Figure 5: Results of grid-spacing sensitivity analyses on a spherical cap (span-to-height ratio = 21.43). For this surface the triangular connectivity is the most sensitive to grid-spacing variations, as its load bearing capacity rockets as grid-spacing increases.

## 6. Results

We have compared the triangular, quadrilateral and statics aware Voronoi-like patterns in terms of buckling strength, compliance and imperfection sensitivity. In particular, the following comparisons have been performed:

**Imperfection sensitivity analysis:** this analysis shows how the buckling factor is affected by surface, grid-topology and imperfections shape, sign and amplitude (see Figure 6 for results and section 3 for the setup of imperfect models).

**'Worst' response diagram *vs* Grid-topology:** for each dataset (first column of Table 1) this study compares the 'worst' response diagram (i.e. that corresponding to the lowest load factor) of each grid-topology (see Figure 7 for results - the state parameter on $x$ axis represents the vertical deflection of the black bullet depicted in Figure 1).

**Response diagram *vs* Imperfection amplitude:** this study outlines the variability of the response diagram with the signed magnitude of the (worst) imperfection shape (see Figure 8 for results). For the sake of brevity, only the results concerning the triangular and statics aware Voronoi remeshings of the *Neumünster* dataset are reported.

### 6.1. *Comparative imperfection sensitivity analysis*

In accordance with Section 1, Figure 6 shows that the triangular topology is definitely the most effective as well as the most sensitive to imperfections (see Figures 6(a) and 6(c)), followed by our statics aware Voronoi remeshing (Figures 6(c) and 6(b)), while the quadrilateral pattern turns out to be the less sensitive to imperfections. These numerical results are in full accordance with the theoretical predictions of Tonelli (18), which where partially sketched in Section 1.

Additionally, it is also evident that the regularity of the surface plays a central role in the definition of the critical point. According to section 5, Neumünster and British Museum datasets represent rather regular geometries (the former more regular than the latter, see Figures 1 and 4) whereas Aquadom and Lilium Tower Top are free-form surfaces. Figures 6(a) and 6(c) show that the Neumünster and British Museum datasets display an *unstable symmetric bifurcation point* (42) (compare the graphs with the two-thirds power law cusp of Figure 6(e)) roughly irrespective of the topology, although the trend is much more noticeable for the triangular topology. Similarly, Figures 6(b) and 6(d) show that free-form surfaces such as Aquadom and Lilium datasets display a *limit point* (42) (compare the graphs with the monotonic non-singular curve of Figure 6(f)), again irrespective of the topology.

Another clear result provided by Figure 6 is that the statics aware Voronoi topology is just as efficient as the quadrilateral topology when the underlying surface is quite regular (Neumünster and British Museum datasets, respectively Figures 6(a) and 6(c)) but its efficiency is even more than twice that of the quadrilateral pattern when the underlying surface becomes irregular or totally free-form (Aquadom and Lilium datasets, respectively Figures 6(b) and 6(d)).

Contrary to polar-symmetric domes (which exhibit a symmetric graph both for negative and positive imperfections (20)), none of the tested grid-shells show a symmetric behaviour with respect to the imperfection sign. Hence, the *sign of imperfections* plays a crucial role in the structural behaviour of grid-shells. Besides, the singularity of the cusp representative of the unstable symmetric bifurcation point of Figures 6(a) and 6(c) does never correspond to the perfect model. This in turn means that the perfect grid-shell does not necessarily produce the highest buckling factor (it never does in our experiments). Therefore, in certain circumstances, a slight imperfection acts as a mild stiffening for the grid-shell.

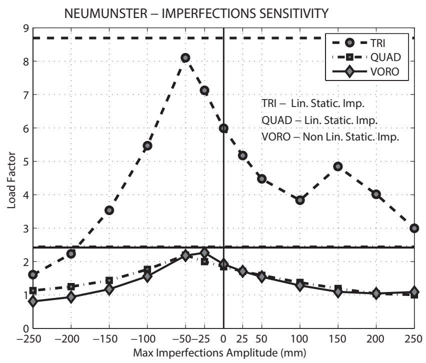


(a) Neumünster

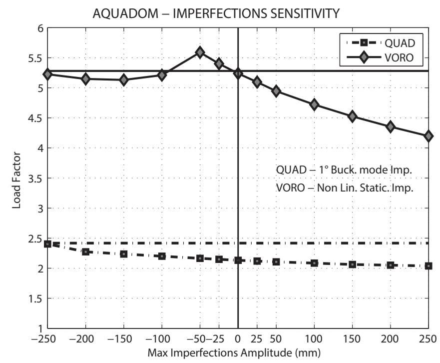


(b) Aquadom

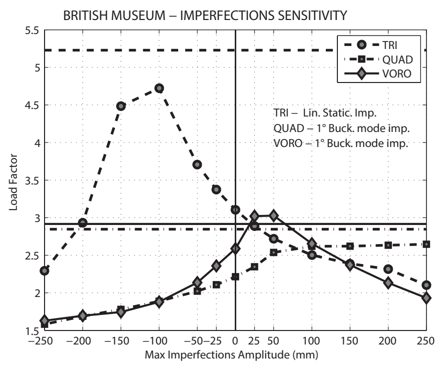


(c) British Museum

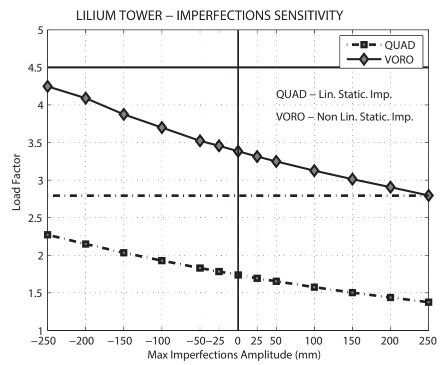


(d) Lilium Tower

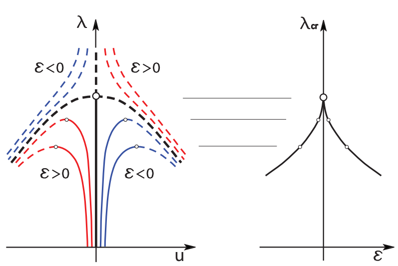


(e) Unstable symmetric bifurcation point

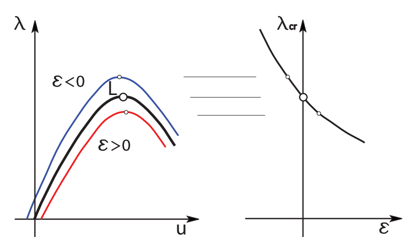


(f) Limit point

Figure 6: Imperfection sensitivity results. On the left column, from top to bottom: *Neumünster Abbey* courtyard glass roof, *British Museum* great court roof and schematic representation of an unstable symmetric bifurcation point. On the right column, from top to bottom: *Aquadom*, *Lilium Tower* and schematic representation of a limit point. The horizontal lines in Figures (a)-(d) represent the first linear eigenvalue (i.e. buckling load) computed on the corresponding perfect model. Text within the graphs of Figures (a)-(d) recalls the 'worst' geometric imperfection shape which generates the graphs (see section 3 for terminology).

As a last remark, at least for uniformly distributed load, the 'worst' imperfection shape is topology-dependent. It is seen that, among the imperfection shapes taken into account (see section 3 for details and terminology), the 'worst' is:

1. the first linear eigenmode $LB$ for triangular topology (see Figures 6(a),(c));
2. either the first linear eigenmode $LB$ or the linear static displacement shape $LS$ for the quadrilateral topology (see Figures 6(b),(c) and 6(a),(d), respectively);
3. the initial buckling shape of the perfect model $NLS$ for the statics aware Voronoi-like topology (see Figures 6(a),(b),(d)).

According to section 3, other convex combinations of linear eigenmodes have been considered, but in no case any of these has come out as the 'worst' imperfection shape. Unfortunately, in agreement with Bulenda and Knippers (20), from our sensitivity analysis no relationship between imperfection shape and amplitude can be worked out, in order to predict the 'worst' imperfection.

### *6.2. Comparative analysis of 'worst' response diagram vs Grid-topology*

Figure 7 shows the 'worst' response diagrams for each grid-topology (i.e. triangular, quadrilateral and statics aware Voronoi-like) of each dataset first column of Table 1). As usual, the term 'worst' response diagram means that it is associated with the imperfect model which produces the lowest load factor.

As expected, triangular grid-shells achieve the highest load factor together with the lowest deformation (see Figures 7(a) and 7(b)). As already outlined in sections 1 and 6.1, the triangular topology is together the strongest as well as the most stiff, to such an extent that it does not require any stiffening device.

On the contrary, almost the totality of the polygonal (i.e. quadrilateral and statics aware Voronoi-like) grid-shells exhibit a very much pronounced softening behaviour prior to collapse. They fail when a local maximum is reached along the primary equilibrium path, but by then they have undergone extremely high (totally unsatisfactory) forerunner displacements. Roughly speaking, they behave like thick equivalent continuous shells made of a 'squashy' material (i.e. with low equivalent Young modulus), according to the analytical results of Tonelli (18). It is worth noticing that this happens irrespective of the regularity of the underlying surface, i.e. there is no distinction between regular datasets such as Neumünster and British

Museum and free-form datasets such as Aquadom and Lilium (just compare the scale of the horizontal axis in Figures 7(a),(b) and 7(d)). These huge displacements point out the need for the adoption of an appropriate stiffening method, aimed at reducing the flexibility. Indeed, polygonal lattice shells exhibit a proper shell behaviour only when a suitable stabilizing system is introduced. Usually a bracing cable system is used that caters for the shear forces to be transferred by membrane action, whereas transverse diaphragms might be added in order to provide for the double curvature to be maintained (17).

Eventually, as already pointed out in section 6.1, the statics aware Voronoi remeshing becomes very effective for architectural free-form surfaces with a high height-to-span ratio (i.e. *Aquadom* and *Lilium Tower* datasets). Indeed, it achieves buckling factors which are on average twice as much as those yielded by equivalent quadrilateral state-of-the-art grid-shells (see Figures 7(c) and 7(d)). This excellent result is due both to the innate adaptivity of the Voronoi diagram and to the *'statics awareness'* introduced by Pietroni et al. (1).

### *6.3. Response diagram vs Imperfection amplitude*

Figure 8 illustrates the variation of the response diagram with the signed amplitude of the imperfection for the Neumünster dataset. For the sake of brevity, only the triangular and statics aware Voronoi-like topologies are reported with reference to their 'worst' imperfection shape (i.e. the *LS* and *NLS* imperfections, respectively - see Figure 6(a)).

It is evident that there is no straightforward correlation between the imperfection amplitude and the shape of the response diagram. It is also worth mentioning that GSA (21) works in load control, which in turn means that it is not able to follow the post-buckling behaviour (e.g. also the potential bifurcation point of the triangular pattern). A correlation is instead spotted between the trend of the diagrams of Figure 8 and those of Figure 6(a). In particular, the cusp points of Figure 6(a) correspond to a sensible snap-back and an almost infinite slope in the corresponding response diagrams of Figures 8(a) and 8(b), respectively. In so doing, the cusp points of Figure 6(a) can be regarded as 'boundary lines' (red lines in Figure 8) in the response diagram *vs* imperfection amplitude graphs of Figure 8.

Eventually, the triangular topology displays a rather linear behaviour up to collapse (or up to the 80% of the collapse load at least) on average. On the

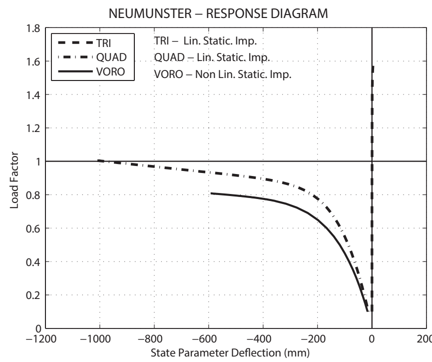


(a) Neumünster

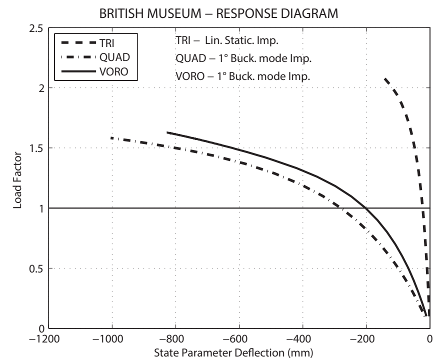


(b) British Museum

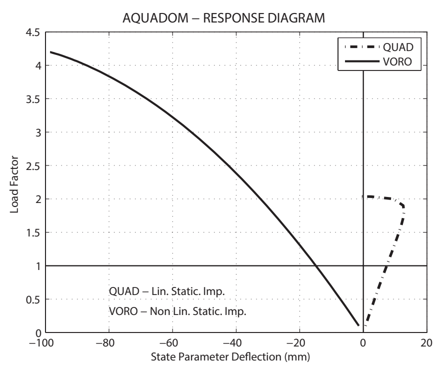


(c) Aquadom

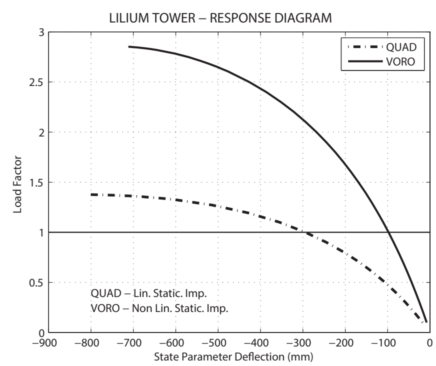


(d) Lilium Tower

Figure 7: ‘Worst’ response diagrams *vs* Grid-topology. Respectively from top left to bottom right: *Neumünster Abbey* courtyard glass roof, *British Museum* great court roof, *Aquadom* and *Lilium Tower* datasets. The horizontal solid lines represent the ‘safety’ unit load factor. Text within the graphs recalls the ‘worst’ geometric imperfection shape which generates the diagrams (see section 3 for terminology). The state parameter referred to on the $x$ axis is the vertical deflection of the black bullet depicted in Figure 1.

contrary, the statics aware Voronoi-like topology exhibits a sensible softening behaviour along the loading process, that intensifies as the imperfection amplitude grows.

Unfortunately, there are no evident rules on how to state in advance the load-deflection relation for a whatsoever imperfect structure. Then the engineer has to undergo all the efforts of a thorough imperfection sensitivity analysis, as the response diagram shape affects the safety of the structure.

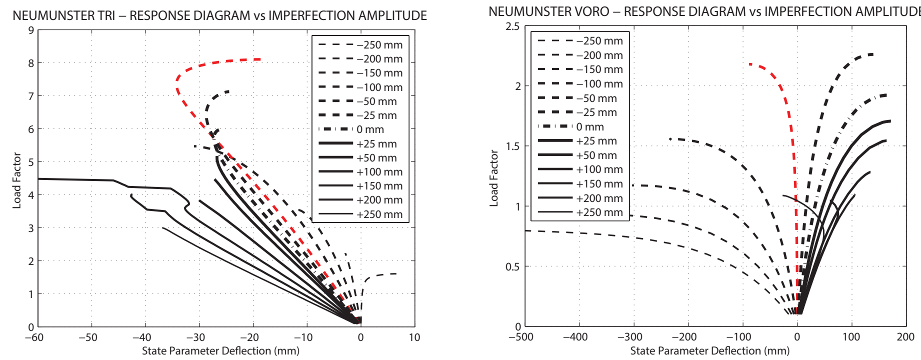


(a) Neumünster Triangular topology

(b) Neumünster statics aware Voronoi-like topology

Figure 8: Variation of the response diagram with the signed amplitude of the imperfection for the *Neumünster* dataset. On the left the triangular remeshing, on the right our statics aware Voronoi remeshing. The state parameter referred to on the $x$ axis is the vertical deflection of the black bullet depicted in Figure 1.

## 7. Statics-Aware Voronoi Mock-up

Building a mock-up and carrying out load tests on it is an opportunity both for appraising the practical feasibility of the statics aware Voronoi remeshing and for validating the numerical results, respectively.

### *7.1. The geometry of the mock-up*

Therefore a mock-up of a funicular Statics Aware Voronoi Grid-Shell was built at the Department D.E.S.T.e.C. of the University of Pisa, with overall dimensions (2.4x2.4x0.7)m and composed of 465 joints, 697 beams and 231 panels (see Figure 9 and Table 2 for statistics). Eventually, incremental static load tests were carried out on it. The joints were 3D printed, the timber beams manually cut and the P.E.T. panels laser cut. All the geometry was digitally handled by means of Rhinoceros (43), in particular using its plug-in RhinoScript for automating some procedures. During the assembling phase (lasted 17 days) temporary ‘scaffoldings’ were needed until the structure was completed and could bear its own weight (see Figure 9). Unfortunately the building process was slowed down by the ABS joints that, being not strong enough to bear the radial tension brought about by the insertion of the rods within the hollow pipes, kept on cracking very often. This in turn has introduced also a significant error in the accuracy of the built geometry, and we assume a maximum deviation (i.e. an imperfection) of about 5 cm from the design geometry.

| | *Beams* | *Joints* | *Faces* | *Washers* | *Screws* |
|---|---|---|---|---|---|
| Number | 697 | 231 | 465 | 227 | 243 |
| Material | Mild Fir | ABS | PET | Iron | Iron |
| $\rho$ ($\frac{kg}{m^3}$) | 400 | 1050 | 1400 | 7750 | 7750 |
| Various | $E = 8$ GPa<br>$L = 72.7$ m<br>$\phi = 8$ mm | $V = 8.4$ dm$^3$<br>Fill $\simeq 20\%$ | $t = 0.8$ mm<br>$A = 5.2$ m$^2$ | t=1.5 mm<br>$\phi_e = 23$ mm<br>$\phi_i = 6$ mm | 3x12 mm |
| $M_{tot}$ (kg) | 1.5 | 1.6 | 7.2 | 2.5 | 0.3 |
| $M_{tot}$ (kg) | 13.1 | | | | |

Table 2: Statistics on the mock-up.

### 7.2. Experimental incremental load test

The apparatus for an incremental statics load test was then set up, as shown in Figure 10. The structure is symmetrically loaded on 16 points (see starred points in Figure 9 (top left)) by hollow metal plates, hung by means of cords with a metal hook at their free end. Each plate weights 120g and each load step provides for the addition of 16 plates (one for each hook), for a total weight of 1.920 kg = 19.20 N. Vertical displacements are monitored at points P1, P2, P3 and P4 (see labeled points in Figure 9 (top left)) by means of 'inductive displacement transducers'. The acquisition system relies on a control unit (HBM WPM 100) endowed with a suitable acquisition software (HBM Catman 3.1) for saving and elaborating the data in real-time. All the instrumentation has been fastened to an external metal scaffolding, in order to avoid any data corruption due to flexibility of the wooden flatbed.

The results were a bit disappointing (see Figure 11 (top)). Although the grid shell is not perfectly symmetric, the underlying surface is and therefore quasi symmetric response diagrams were expected for the four monitored points. Instead, Figure 11 (top) clearly shows two main different trends: the 'left' nodes (i.e. P1 and P2) undergo a non negligible displacement, whereas 'right' nodes (i.e. P3 and P4) stay almost steady during the whole load process. Additionally, all nodes display a remarkable irreversible deformation after the unloading has occurred.

The joints were given credit for most part of this behaviour, as they actually act like almost compression-only constraints, while only a small (but highly scattered and unpredictable) amount of tension can be carried through friction. In particular it was deemed that, under loading, some partially inserted rods might have slid deeper into the hollow pipes, while some other fully inserted may have slid out of their slots. Hence, two additional and identical load tests were scheduled, in order to pin down the real behaviour of the mock-up by gradually phasing the joints non-linearity out. Figures 11 (middle) and 11 (bottom) show the results of the second and third load tests, respectively. The second test seem to be the most reliable among all, as all monitored points display a similar softening behaviour. Nevertheless, significant irreversible displacements are still experienced at the unloaded state. On the other hand, the results of the third test show a significant change in the behaviour of the 'right' nodes (i.e. P3 and P4), which means that some swing has happened within the grid-shell, probably due to the cracking of some joints, to some rods having lost contact with their pertaining nodes or to some large scale permanent modification having occurred to the overall geometry of the grid shell. The first and last considerations are definitely supported by Figure 10 (bottom row), that shows the mock-up after the third and last static test had been carried out on it. It is evident how the shape is now affected by significant changes in curvature, while some nodes have slid out of their housing. Ultimately, we can say that the structure has buckled by the repeated application of the same load.

### *7.3. Calibrated numerical tests*

Actually the behaviour of the mock-up turns out to be quite complex and far from being symmetric as the pseudo-symmetry of the structure would indicate. In particular, the following sources of non-linearity steer its static response:

1. high deformability of the structure (geometrical non-linearity);
2. joints cracking (material non-linearity);
3. monolateral restraints at the joints, i.e. sliding of rods within the joints' hollow pipes (contact non-linearity).

Within the FE-program GSA (21) we can model geometrical non-linearity by simply carrying out geometrically non-linear analyses. We might also partially model the material non-linearity (i.e. we could set up an equivalent

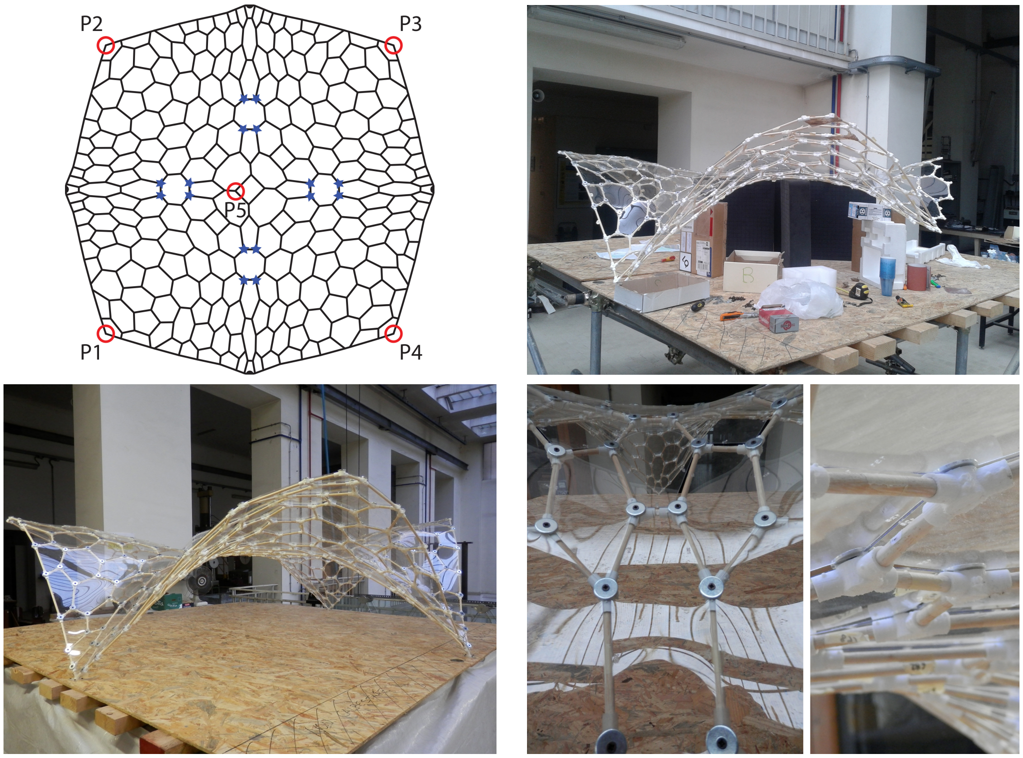


Figure 9: The geometry of the Statics Aware Voronoi Grid-Shell mock-up.

non-linear material, but not directly model the cracks) and the contact non-linearity (i.e. we could use compression-only elements for the joints, but not directly model the friction), although it would require a lot of expertise and plenty of time for the calibration. Such a detailed study is out of the scope of the paper, thus we contented ourselves with a sensitivity analysis carried out by means of geometrically non-linear analyses only, as already done in section 6. We adopted the same imperfection shapes described in section 3 (i.e. *LS*, *LB* and *NLS*) and we scale them by varying the maximum norm in the discrete range $\pm[100\ 75\ 50\ 25\ 12.5\ 0]$ mm, thus obtaining a total of 33 imperfect models.

Figure 12 shows the results of this analysis: it is seen that the critical point is imperfection shape dependent. In particular an unstable symmetric bifurcation point appears with the first linear eigenmode *LB* and the initial buckling shape *NLS*, whereas a limit point is associated with the linear static displacement shape *LS*. As already noticed in section 6.1, also in this case the

Figure 10: The static incremental load test on the Statics Aware Voronoi Grid-Shell mock-up. From top left to bottom right: setup, loading phase and large permanent changes in shape after the third load test.

*NLS* imperfection shape yields almost the most unfavourable buckling loads (at least for small amplitudes). Contrarily to section 6.1 instead, the cusp is centered on the zero amplitude, i.e. it is associated with the perfect model. This result might be related to the funicularity of the surface underlying the Statics Aware Voronoi Grid-Shell mock-up.
Unfortunately, by simply comparing the scale of the y-axis of Figure 12 with that of Figure 11 displaying the experimental load tests results, it is immediately observed how poorly the numerical model describes the real behaviour of the mock-up. Apparently the effect of material and contact non-linearities is not negligible, as witnessed by the lowest numerical buckling load being twice as big as the experimental load. For the sake of clarity, 7 is not properly the buckling factor of the mock-up as the loading process was stopped before reaching collapse in order to spare the model, but probably the real

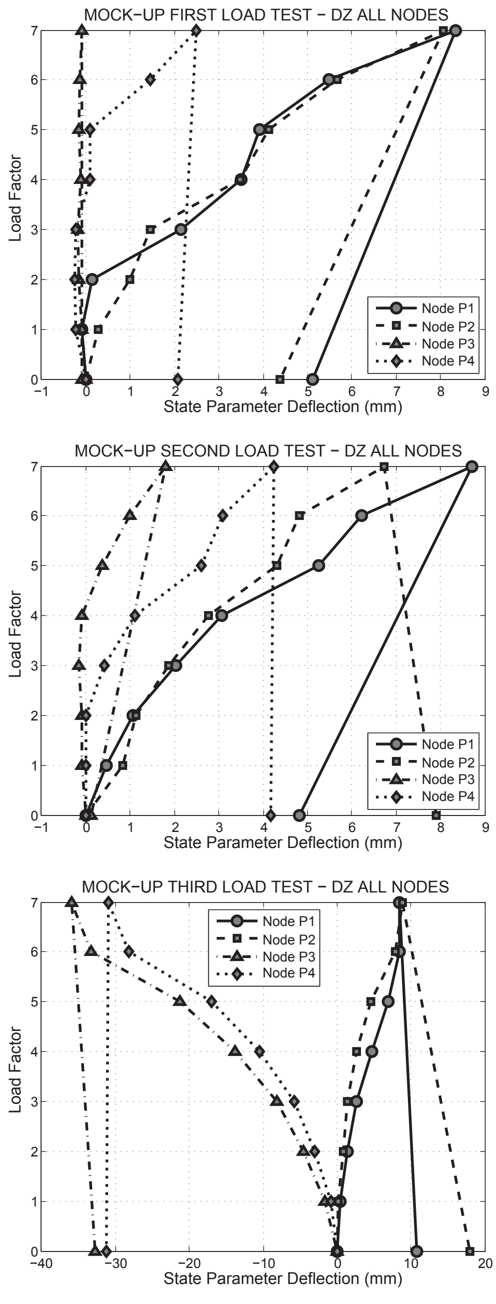


Figure 11: Experimental response diagrams for all monitored nodes P1, P2, P3 and P4. From top to bottom: first, second and third load tests, respectively.

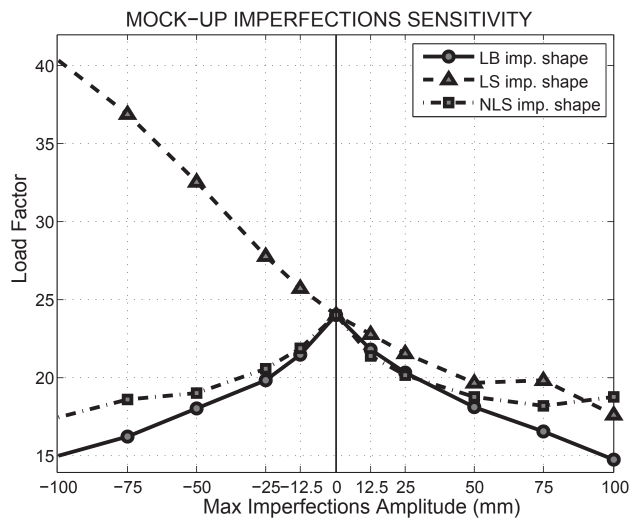


Figure 12: Imperfection sensitivity of the Statics Aware Voronoi Grid-Shell mock-up.

buckling load was about no more than 10.

## 8. Conclusions

This paper evaluates the structural performances of a novel hex-dominant remeshing pattern for free-from grid-shells: the *Statics Aware Voronoi Remeshing* scheme introduced by Pietroni et al. (1). The basic intuition is to lay out the beams network along the edges of an anisotropic centroidal Voronoi tessellation of the surface, where the metric used is not the Euclidean metric but that induced by the stress tensor over the surface under uniform load.

In order to assess the structural capabilities of the Statics Aware Voronoi Grid-Shells, we have carried out a systematic comparative analysis between them and equivalent state-of-the-art competitors (i.e. grid-shells with triangular and quadrilateral topology). To this aim, we have performed extensive investigations through numerical geometrically non-linear analyses. The results we have obtained show that our free-form Statics Aware Voronoi Grid-Shells are not only aesthetically pleasing but also statically efficient. Obviously they cannot be as efficient as the triangular grid-shells, but they turn out to be twice as effective as their equivalent state-of-the-art quadrilateral competitors. Therefore they represent indeed a valid alternative for the design of modern grid-shells, especially if the underlying surface is free-form.

In particular we have observed that the bigger the geometry irregularity of the underlying surface, the better the structural performances of our Statics Aware Voronoi Grid-Shells, thanks to the *statics awareness* supplied by the statically driven metric.

A thorough imperfection sensitivity analysis has also been carried out. We have found out that the 'worst' imperfection shape is topology-dependent, i.e. it varies with the remeshing pattern even if the underlying surface is kept constant. In particular, the initial buckling shape proposed by Schneider (25; 35) under the name of 'quasi-collapse-affine' imperfection, seems to be the most unfavourable imperfection for the Statics Aware Voronoi Grid-Shells. Additionally, although less sensitive to imperfections than their 'brothers' shells, the reduction of the buckling load might be very high also for grid-shells. Specifically, the failure load can be even four times lower for triangular and highly regular grid-shells, whereas the minimum load bearing capacity erosion due to geometrical imperfections is not less than 30% for Statics Aware Voronoi Grid-Shells. Eventually, in some circumstances, the quadrilateral topology exhibits an even lower sensitivity (see Figure 6).

From a geometrical and pragmatic standpoint, statics aware Voronoi meshes have twice the number of vertices with respect to statically equivalent quadrilateral meshes (see section 5.2), but at the same time all vertices have valence three (see Table 1), thus they are competitive from the feasibility viewpoint too. For issues such as planarity of the faces and further details about the geometry, the reader is referred to (1).

Eventually a mock-up of a Statics Aware Voronoi Grid-Shell has been built in order to assess the inherent complexities of this innovative lightweight structure. Load tests performed on it have confirmed the general knowledge that the behaviour of a real grid-shell is hard to describe with numerical models only.


[1] N. Pietroni, D. Tonelli, E. Puppo, M. Froli, R. Scopigno, P. Cignoni, Statics Aware Grid Shells, Computer Graphics Forum (To appear).

[2] W. Koiter, On the stability of elastic equilibrium, NASA technical translation, National Aeronautics and Space Administration, 1967.

[3] J. W. Hutchinson, Imperfection sensitivity of externally pressurized spherical shells, Journal of Applied Mechanics 34 (1967) 49–55.

[4] V. Gioncu, Buckling of Reticulated Shells: State-of-the-Art, International Journal of Space Structures 10 (1995) 1–46.

[5] S. P. Timoshenko, J. M. Gere, Theory of elastic stability, McGraw-Hill classic textbook reissue, McGraw-Hill, 1988, New York, 1961, reprint. Originally published: 2nd ed. New York : McGraw-Hill, 1961. (Engineering societies monographs).

[6] V. I. Weingarten, P. Seide, J. P. Peterson, Buckling of thin-walled circular cylinders, Tech. rep., NASA (1968).

[7] D. T. Wright, Membrane forces and buckling in reticulated shells, Journal of the Structural Division 91 (1) (1965) 173–202.

[8] S. E. Forman, J. W. Hutchinson, Buckling of reticulated shell structures, International Journal of Solids and Structures 6 (7) (1970) 909 – 932. doi:http://dx.doi.org/10.1016/0020-7683(70)90004-1.

[9] J. Sumec, A. Zingali, A study of the influence of initial shape imperfections on the stability of lattice shells by direct and shell analogy method., International journal of space structures 2 (1987) 223–230.

[10] S. Adriaenssens, P. Block, D. Veenendaal, C. Williams (Eds.), Shell Structures for Architecture: Form Finding and Optimization, Taylor and Francis - Routledge, London, 2014.

[11] S. Malek, C. J. K. Williams, Structural implications of using cairo tiling and hexagons in gridshells, Wroclaw, Poland, 2013, proceedings of the International Association for Shell and Spatial Structures (IASS) Symposium 2013 - "Beyond the Limits of Man".

[12] J. Schlaich, H. Schober, Glass-covered lightweight spatial structures, 1994, pp. 1–27.

[13] J. Schlaich, H. Schober, Glass-covered grid-shells, Structural Engineering International: Journal of the International Association for Bridge and Structural Engineering (IABSE) 6 (2) (1996) 88–90.

[14] J. Schlaich, H. Schober, Glass roof for the hippo house at the berlin zoo, Structural Engineering International: Journal of the International Association for Bridge and Structural Engineering (IABSE) 7 (4) (1997) 252–254.

[15] J. Glymph, D. Shelden, C. Ceccato, J. Musse, H. Schober, A parametric strategy for free-form glass structures using quadrilateral planar facets, Automation in Construction 13 (2004) 187–202.

[16] Y. Liu, H. Pottmann, J. Wallner, Y.-L. Yang, W. Wang, Geometric Modeling with Conical Meshes and Developable Surfaces, ACM Transactions on Graphics 25 (2006) 681–689.

[17] J. Schlaich, H. Schober, Design principles of glass roofs, 2002, pp. 815–827, proceedings of the International Symposium on Lightweight structures in civil engineering, Warsaw, Poland.

[18] D. Tonelli, Statics Aware Voronoi Grid-Shells, Ph.D. thesis, University of Pisa (2014).

[19] C. Jiang, J. Wang, J. Wallner, H. Pottmann, Freeform honeycomb structures, Computer Graphics Forum 33 (5), Proc. Symp. Geom. Processing.

[20] T. Bulenda, J. Knippers, Stability of grid shells, Computers and Structures 79 (12) (2001) 1161 – 1174. doi:http://dx.doi.org/10.1016/S0045-7949(01)00011-6.

[21] Oasys Software, GSA Version 8.6 reference manual., Arup, 13 Fitzroy Street London. (2012).

[22] H. Schmidt, Stability of steel shell structures: General report, Journal of Constructional Steel Research 55 (13) (2000) 159 – 181. doi:http://dx.doi.org/10.1016/S0143-974X(99)00084-X.
URL `http://www.sciencedirect.com/science/article/pii/S0143974X9900084X`

[23] D. Dinkler, J. Pontow, A model to evaluate dynamic stability of imperfection sensitive shells, Computational Mechanics 37 (6) (2006) 523–529. doi:10.1007/s00466-005-0729-7.
URL `http://dx.doi.org/10.1007/s00466-005-0729-7`

[24] E. Ewert, K. Schweizerhof, P. Vielsack, Measures to judge the sensitivity of thin-walled shells concerning stability under different loading conditions, Computational Mechanics 37 (6) (2006) 507–522. doi:10.1007/s00466-005-0733-y.
URL `http://dx.doi.org/10.1007/s00466-005-0733-y`

[25] W. Schneider, I. Timmel, K. Hhn, The conception of quasi-collapse-affine imperfections: A new approach to unfavourable imperfections of thin-walled shell structures, Thin-Walled Structures 43 (8) (2005) 1202 – 1224. doi:http://dx.doi.org/10.1016/j.tws.2005.03.003.
URL `http://www.sciencedirect.com/science/article/pii/S0263823105000583`

[26] M. Deml, W. Wunderlich, Direct evaluation of the "worst" imperfection shape in shell buckling, Computer Methods in Applied Mechanics and Engineering 149 (14) (1997) 201 – 222.

[27] D. Ho, The influence of imperfections on systems with coincident buckling loads, International Journal of Non-Linear Mechanics 7 (3) (1972) 311 – 321. doi:http://dx.doi.org/10.1016/0020-7462(72)90053-4.
URL `http://www.sciencedirect.com/science/article/pii/0020746272900534`

[28] R. Greiner, P. Derler, Effect of imperfections on wind-loaded cylindrical shells, Thin-Walled Structures 23 (14) (1995) 271 – 281, buckling Strength of Imperfection-sensitive Shells. doi:http://dx.doi.org/10.1016/0263-8231(95)00016-7.
URL `http://www.sciencedirect.com/science/article/pii/026382319500016 7`

[29] E. Lindgaard, E. Lund, K. Rasmussen, Nonlinear buckling optimization of composite structures considering worst shape imperfections, International Journal of Solids and Structures 47 (2223) (2010) 3186 – 3202. doi:http://dx.doi.org/10.1016/j.ijsolstr.2010.07.020.
URL `http://www.sciencedirect.com/science/article/pii/S0020768310002738`

[30] CEN, Eurocode 3: Design of Steel Structures. Part. 1-6: Strength and Stability of Shell Structures, CEN, 2007, `https://law.resource.org/pub/eur/ibr/en.1993.1.6.2007.html`.

[31] C. Graciano, E. Casanova, J. Martnez, Imperfection sensitivity of plate girder webs subjected to patch loading, Journal of Constructional Steel Research 67 (7) (2011) 1128 – 1133. doi:http://dx.doi.org/10.1016/j.jcsr.2011.02.006.
URL `http://www.sciencedirect.com/science/article/pii/S0143974X11000459`

[32] N. Kristani, J. Korelc, Optimization method for the determination of the most unfavorable imperfection of structures, Computational Mechanics

42 (6) (2008) 859–872. doi:10.1007/s00466-008-0288-9.
URL http://dx.doi.org/10.1007/s00466-008-0288-9

[33] C. Song, J. Teng, J. Rotter, Imperfection sensitivity of thin elastic cylindrical shells subject to partial axial compression, International Journal of Solids and Structures 41 (2425) (2004) 7155 – 7180. doi:http://dx.doi.org/10.1016/j.ijsolstr.2004.05.040.
URL http://www.sciencedirect.com/science/article/pii/S0020768304002756

[34] W. Schneider, A. Brede, Consistent equivalent geometric imperfections for the numerical buckling strength verification of cylindrical shells under uniform external pressure, Thin-Walled Structures 43 (2) (2005) 175 – 188. doi:http://dx.doi.org/10.1016/j.tws.2004.08.006.
URL http://www.sciencedirect.com/science/article/pii/S0263823104001648

[35] W. Schneider, Stimulating equivalent geometric imperfections for the numerical buckling strength verification of axially compressed cylindrical steel shells, Computational Mechanics 37 (6) (2006) 530–536. doi:10.1007/s00466-005-0728-8.
URL http://dx.doi.org/10.1007/s00466-005-0728-8

[36] Q. Du, V. Faber, M. Gunzburger, Centroidal Voronoi Tessellations: Applications and Algorithms, SIAM Review 41 (4) (1999) 637–676. doi:10.1137/S0036144599352836.
URL http://epubs.siam.org/doi/abs/10.1137/S0036144599352836

[37] M. Corsini, P. Cignoni, R. Scopigno, Efficient and flexible sampling with blue noise properties of triangular meshes, IEEE Transactions on Visualization and Computer Graphics 18 (6) (2012) 914–924.

[38] S. Valette, J.-M. Chassery, Approximated Centroidal Voronoi Diagrams for Uniform Polygonal Mesh Coarsening, Computer Graphics Forum 23 (3) (2004) 381–389. doi:10.1111/j.1467-8659.2004.00769.x.
URL http://doi.wiley.com/10.1111/j.1467-8659.2004.00769.x

[39] RFR-Paris, Neumünster abbey glazing, neumünster luxembourg (2003).

[40] C. J. K. Williams, The analytic and numerical definition of the geometry of the british museum great court roof, Deakin Unversity, Geelong, Australia, 2001, pp. 434–440, proceedings of the Third International Conference on Mathematics & Design, M&D.

[41] E. Vouga, M. Höbinger, J. Wallner, H. Pottmann, Design of self-supporting surfaces, ACM Trans. GraphicsProc. SIGGRAPH.

[42] J. Thompson, G. Hunt, Elastic Instability Phenomena, 1st Edition, John Wiley & Sons, Inc., New York, NY, USA, 1984.

[43] M. Becker, P. Golay, Rhino NURBS 3D Modeling, no. v. 1, New Riders, 1999.